AIAA AVIATION Forum
June 15-19, 2020, VIRTUAL EVENT
AIAA AVIATION 2020 FORUM

10.2514/6.2020-2920

A Simulated Wind-field Dataset for Testing Energy Efficient Path-Planning Algorithms for UAVs in Urban Environment

Deepika Baskar* and Alex Gorodetsky†
University of Michigan, Ann Arbor, Michigan, 48105

Managing winds in the urban wind environment is an important aspect for enabling efficient wide-spread autonomous drone activity in urban centers. Literature studying the effects of wind on urban air mobility in a realistic urban geometry is emerging and typically requires comprehensive fluid dynamics simulations. However, the accessibility of these approaches to those with less fluid dynamics experience and/or without access to purpose built simulation tools has limited validation and application of the corresponding results. This paper seeks to address this issue by describing a set of wind simulations in a real urban environment that we have made openly available to the community. Our aim is to increase the feasibility of using fluid dynamics simulation for testing UAV strategies in the urban environment. As an example application, we use our dataset to determine energy optimal paths for a hypothetical fixed-wing UAV tasked with making trips spanning a few city blocks. We demonstrate that energy efficiency considerations can indeed lead to different path planning results than those used by conventional shortest path planners, and therefore may be an important factor when designing UAV operations.

I. Nomenclature

$\vec{a}$	=	Vector along the present node to the next waypoint of the flight path, m
AR	=	Wing aspect ratio
$\hat{\vec{b}}$	=	Unit vector along the present node to the goal, m
$C_{D,0}$	=	Parasitic Drag coefficient
d	=	Dimension of the free space
D	=	Drag, N
e	=	Oswald efficiency factor
e_a	=	Relative error
e_{ext}	=	Extrapolated relative error
E	=	Set of edges
$\dot{E}_a$	=	Air relative power
g	=	Acceleration due to gravity, m/s^2
G	=	Graph generated using PRM^* algorithm
K_e	=	Weighting constant on the drag energy component of the cost function
K_{nav}	=	Weighting constant on the energy to goal component of the cost function
J_w	=	Spatial wind gradient
L	=	Lift, N
$(\frac{L}{D})_{est}$	=	Approximate glide ratio for distance reward function
m	=	Mass of the UAV, kg
n	=	Number of edges connected to the present node
N_i	=	Mesh at i^{th} refinement
p	=	Local order of accuracy
$r(n)$	=	Ball radius
r_p	=	Grid refinement factor
$\vec{R}$	=	Ground Speed, m/s^2

*Graduate Student, Department of Aerospace Engineering, University of Michigan, Ann Arbor, MI - 48105, AIAA Student Member
†Assistant Professor, Department of Aerospace Engineering, University of Michigan, Ann Arbor, MI - 48105, AIAA Member

V	=	Set of vertices in the free space
$\vec{V_a}$	=	Relative airspeed, m/s^2
$\vec{W}$	=	Wind field vector
$\mu(\chi_{free})$	=	Lebesgue measure of the obstacle-free space χ_{free}
γ	=	Pitch Angle, deg
ϕ	=	Roll angle, deg
ψ	=	Heading angle, deg
θ_i	=	Field variable considered
ζ_d	=	Volume of unit ball in euclidean space

II. Introduction

With dozens of companies recently joining the race for Urban Air Mobility [1], the demand to develop safe and energy efficient paths for autonomous unmanned aerial vehicles (UAVs) is rapidly becoming a critical issue in wide ranging civilian and military applications [2]. In these applications, energy efficiency can be gained, not only through the development of efficient new battery systems, but also through more efficient path planning. Specifically, the complex flow physics existing in urban environments can have a tremendous impact on the capabilities and operations of UAVs [3].

Determining, to a first order approximation, these specific effects can be done by first developing computational simulations of the flow physics in relevant environments, and then simulating the flight of an aircraft through these flows. Simulations of the interaction between the aircraft and the environment can then demonstrate significant impacts on the energy efficiency depending on the path it traverses through the flow. For example, extracting energy from the environment is a prime goal for static and dynamic soaring and has numerous applications to both air travel and energy generation [4]. The concept of dynamic soaring, a common phenomena displayed by migrating albatrosses to extract energy form the wind field using Rayleigh cycle [5], is used to obtain energy efficient paths by exploiting the energy gain boundary layers and updrafts present in a windy environment. Moreover, advantageously traversing through these updrafts can significantly improve endurance of UAVs [6].

These ideas have also been considered in the context of planning minimum energy trajectory planning for UAVs [3, 6–11]. For example, the works by Orr et.al [7] and Galway et.al [3] approach the problem by considering the wake regions behind the buildings. They seek locations in the wake that most affect the flight of the helicopter and show that the assumption of a constant wind-field is insufficient to capture the details of the flight path. However, the wake interpretation was done only for flows behind up to two buildings and more complex conditions can add adverse effects on UAVs. In the context of improving the endurance of the flight by soaring, Allen [6] suggests the need for a highly reliable low - altitude simulated paths that could be treated as an alternative to real time testing. However, the method comes with the computational penalty of 3D simulation of large three dimensional space infested with complex flow physics. Moreover, there is no availability of the underlying simulation data for other practitioners.

Despite proving to deliver promising outcomes in improving the energy efficiency, the usage of dynamic soaring and other energy-generating maneuvers in minimum energy path planning suffers some practical issues. For instance, to create an optimal path to a target, a complete three dimensional wind field data (mostly from simulation) is required. Furthermore, these simulations are computationally costly and difficult to execute when planning has to be done for longer ranges and for regions with high uncertainty in the location and magnitude of updrafts and gusts.

This paper provides two primary contributions as follows:

1) We describe an open flow simulation source data set containing the wind profile information for the region under study that is contributed to a repository in the Deep Blue Data, managed by The University of Michigan Library [12].
2) We demonstrate energy efficient path planning through an urban environment using the above mentioned data set.

As most of UAV flight time flight time will likely be at an approximately fixed altitude, the computational simulations focused on solving 2D Navier Stokes Equations. These simulations were validated using wind field data made available by the National Weather Services [13]. An ensemble of simulations were carried out over a range of free stream Mach numbers and heading angles. Energy optimal path planning was then performed using a probabilistic roadmap (PRM) planning algorithm.

A. Related Work

Our approach closely builds on two existing contributions: that of Ware and Roy [9] and that of Lawrance and co-authors [8]. Ware and Roy considered the behavior of a quadcopter in a simulated three dimensional wind field using QUIC-CFD, a lightweight CFD solver developed at Los Alamos National Labs [14] from which they extracted two dimensional flow data at a fixed height. They then devised a cost function for penalizing energy intensive paths. This cost function was a combination of kinetic energy, potential energy, and the amount of battery power consumed during the flight, and it was validated by experimental testing (model dependent). Using this cost function, optimal paths were developed through an area of MIT using an A^* algorithm.

The present paper follows this same strategy, but is distinct in two primary ways. First we use a more general purpose simulation tool SU2 [15], which allows us to generate and create open source data for use by the community. Second we consider a different energy formulation that can be applied to fixed wing aircraft.

This alternative methodology adapts the work of Lawrance and co-authors to the present case [8], where a cost function derived by dynamic soaring considerations was created. In that work, a 6DOF aircraft model is considered where thermal updrafts act as lift producing agents that are preceded by the increase in the pitching moment. With this knowledge of the flow physics, they employed an RRT* algorithm to come up with energy efficient paths. While we use essentially the same energy formulation, this work considers an urban environment and uses a more realistic simulation scenario.

B. Organization

The paper is organized as follows: Section III introduces the reader to background on energy efficient path planning and our chosen shortest path simulation. Section IV.A describes the computational flow simulation of a portion of Boston environment. Specifically, we describe the flow domain selection, solver physics grid independent study, and model validation. Section V provides path planning results where we demonstrate that energy efficient paths that consider the flow in the environment can be superior to purely shortest paths.

III. Background and Methods

In this section, we provide background for energy efficient path planning for fixed-wing vehicles.

A. Energy Equations

This sections introduces the reader to the force and energy equations that are used to derive the power expenditure of a glider modeled using 6DOF dynamics. These equations are summarized from [8].

The spatial wind gradient at a point $X = (x, y, z)$ with wind field vector $\vec{W} = [W_x, W_y, W_z]^T$ is given by

$$J_w = \begin{bmatrix} \frac{\partial W_x}{\partial x} & \frac{\partial W_x}{\partial y} & \frac{\partial W_x}{\partial z} \\ \frac{\partial W_y}{\partial x} & \frac{\partial W_y}{\partial y} & \frac{\partial W_y}{\partial z} \\ \frac{\partial W_z}{\partial x} & \frac{\partial W_z}{\partial y} & \frac{\partial W_z}{\partial z} \end{bmatrix}. \tag{1}$$

The relative air speed is

$$\vec{V_a} = \begin{bmatrix} V_a \cos\psi \cos\gamma \\ V_a \sin\psi \cos\gamma \\ -V_a \sin\gamma \end{bmatrix}, \tag{2}$$

and the ground speed is

$$\vec{R} = \vec{V_a} + \vec{W}. \tag{3}$$

The lift generated by an aircraft traveling at speed $\vec{R}$ due to change in climb angle rate and wind gradient J_w is given by

$$L = \frac{m}{\cos\phi}\left(V_a \frac{d\gamma}{dt} + g\cos\gamma - \begin{bmatrix} \cos\psi\cos\gamma \\ \sin\psi\sin\gamma \\ \cos\gamma \end{bmatrix}^T J_w \vec{R} \right), \tag{4}$$

Algorithm 1 PRM* [16]

$V \leftarrow \{x_{init}\} \cup \{SampleFree_i\}_{i=1,\ldots,n}; E \leftarrow \emptyset;$
for each $v \in \mathcal{V}$ **do**
  $U \leftarrow \text{Near}(G = (V, E), v, \gamma_{PRM}(log(n)/n)^{1/d})\{v\};$
  for each $u \in \mathcal{U}$ **do**
    if CollisionFree(v, u) **then**
      $E \leftarrow E \cup \{(v, u), (u, v)\}$
    end if
  end for
end for
return $G = (V, E)$

and the drag is decomposed into parasitic and induced drag

$$D = \frac{1}{2}\rho V_a^2 S C_{D,0} + \frac{L^2}{\frac{1}{2}\rho V_a^2 S \pi A R e}. \tag{5}$$

For the purposes of simulations in Section V, we follow the work by Lawrance [8] and use the parameters $m = 5.44kg$, $S = 0.857m^2$, $AR = 19.54$, $e = 0.85$ and $C_{D,0} = 0.012$.

Given these forces, the air-relative power can be written as a combination of energy gain/loss due to drag, vertical wind component and soaring due to wind gradient:

$$\frac{\dot{E}_a}{m} = -V_a \frac{D}{m} - gW_z - V_a \begin{bmatrix} \cos\psi\cos\gamma \\ \sin\psi\cos\gamma \\ -\sin\gamma \end{bmatrix}^T J_w \vec{R} \tag{6}$$

The air-relative power serves as the basis for computing the energy efficiency of flight paths. It is incorporated into a shortest path planner described next.

B. Path planning and cost function formulation

The primary test case for demonstrating the use of our simulations will be energy efficient path planning. To this end, we describe our probabilistic roadmap approach. We model a scenario where UAVs are required to fly over the roadways of a city. As a result, we sample all legal paths in the city and generate a weighted graph that consists of only legal routes using probabilistic road maps. The weights are chosen to be first order approximations of the energy Equation (6) for a UAV flying at a fixed ground speed.

The legal routes must navigate the roadway geometry shown in Figure 2. We use the PRM* [16] approach to generate the edges of the graph, and Algorithm 1 provides the pseudocode of this approach. Here $\gamma^*_{PRM} = 2(1 + 1/d)^{\frac{1}{d}}(\mu(\chi_{free})/\zeta_d)^{\frac{1}{d}}$ and $r(n) = \gamma_{PRM}(log(n)/n)^{1/d}$ wherein the $r(n)$ is updated every time a new edges gets added to the node.

After generating the graph using PRM*, we assign weights to each edge. These weights are based on Equation (6). Since we consider a 2D computationally simulated environments for planning, the wind gradients acting along z direction are ignored. Additionally, the motion of the vehicle is restricted to only yawing and rolling moments. Together we impose $W_z = 0$, $\frac{\partial W_x}{\partial z} = 0$, $\frac{\partial W_y}{\partial z} = 0$ and $\gamma = 0$.

Following [8], the weight of the path consists of two components: an energy based reward and a navigation reward. The energy based reward

$$R_{\text{energy}} = -mg\left(z_{i,\text{final}} - z_{i,\text{initial}}\right) + \frac{1}{2}m\left(V^2_{a,\text{final}} - V^2_{a,\text{initial}}\right) + K_e E_a \Delta t \tag{7}$$

is composed of three components: the kinetic energy gained/lost during the flight between initial and final nodes; the potential energy gained/lost during the flight between the two nodes; and the air relative power as given by(6) gained/lost. The weight K_e can be chosen arbitrarily (here, $K_e = 0.5$) based on the objective of the problem.

The navigation reward

$$R_{nav} = -mg\frac{\vec{a}\cdot\hat{\vec{b}}}{(\frac{L}{D})_{est}} \tag{8}$$

is the reward incurred during flight between two nodes. As shown in Figure 1, this reward is proportional to the projection of the vector along the direction of flight ($\vec{a}$) over the unit vector onto the line joining the current node and the goal node ($\hat{\vec{b}}$) as seen in Figure.1.

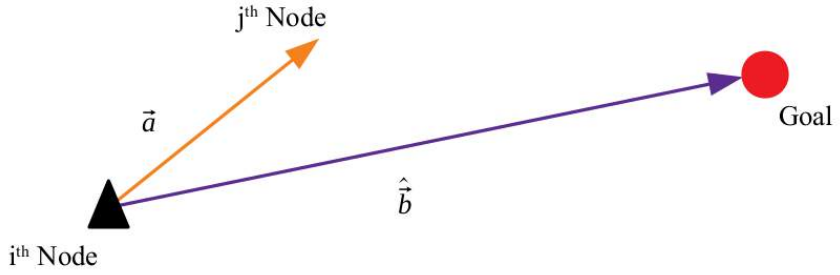

Fig. 1 The figure shows the flight path of the UAV between the nodes i (black triangle) and j as $\vec{a}$ and the unit vector $\hat{\vec{b}}$ connecting the start to the goal (red circle).

These two rewards are combined into a single switching reward function

$$R = \begin{cases} (1-K_{nav})\,R_{\text{energy}} + K_{\text{nav}}R_{\text{nav}} & \text{if } E_{\text{current}} > E_{\text{goal}} + mg|\bar{b}|/\left(\frac{L}{D}\right)_{\text{est}} \\ K_{\text{nav}}R_{\text{energy}} + (1-K_{\text{nav}})\,R_{\text{nav}} & \text{if } E_{\text{current}} \le E_{\text{goal}} + mg|\bar{b}|/\left(\frac{L}{D}\right)_{\text{est}} \end{cases} \tag{9}$$

that is used to weigh the edges in the graph generated. This reward is a combination of energy gained from the flight and the navigation energy weighted by the constant K_{nav}. The function shifts the weights on these two components of energy by using two parameters, $E_{current}$, the air-relative power required to travel from nodes i to j and E_{goal}, the air-relative power required to travel from the present node to goal.

Following the assignment of weights, we construct a shortest path using Dijkstra's algorithm.

IV. Dataset Generation of Urban Flow

This section describes a dataset generated in an urban environment shown in Figure 2.

A. Flow domain and grid generation

Our chosen flow domain is a region in the city of Boston around the coordinates 42°15′17.9"N and 71°08′27.7"W. We found that simulation of the flow physics in this region exhibits significant variation in local velocity direction and magnitude, and thus can potentially serve as a useful test scenario for UAM studies. The CAD footprints for the region are made available by the Boston Planning and Development Agency [17]. The extracted geometry of the region chosen is rendered using commercially available Autocad package [18].

A two dimensional unstructured grid is generated for the region of study using Pointwise software [19] as shown in Figure 3. We followed the guidelines proposed by the Architectural Institute of Japan [20] for practical applications of CFD to pedestrian wind environment around buildings [20] during the design of the grid. Specifically, the domain length is designed sufficiently large to forestall the influence of the boundary over the field variables and to visualize the complete formation of downstream flow. According to the guidelines, the recommended minimum grid resolution is $1/10^{th}$ of the building scale, and the aspect ratio of the cell must not rapidly increase near the walls or the surfaces of complicated geometries. Additionally, prism layering is done near the walls of the buildings to accurately capture separating flows and vortices.

(a) Google Earth view of the region in the city of Boston chosen for study.

(b) Two dimensional Autocad rendering of the city blocks.

(c) Streamlines plot of the wind field flowing from 70° south-west.

Fig. 2 Figures (a) , (b) and (c) denote the stages involved in the CFD simulation for the region under study (left to right).

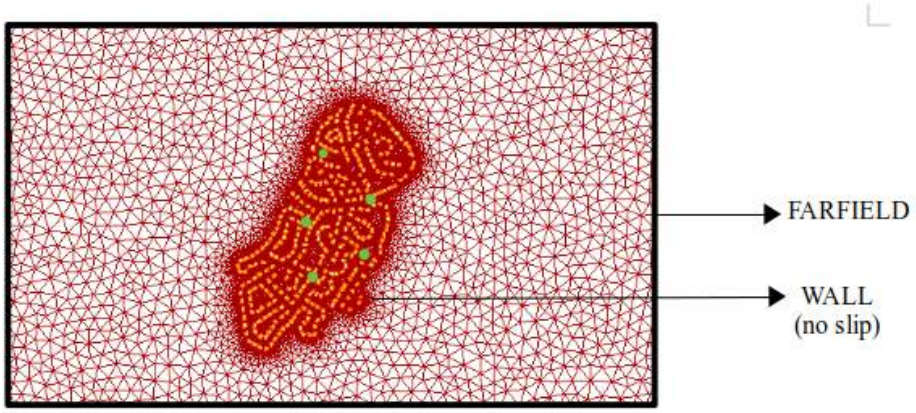

Fig. 3 Grid developed using Pointwise software where the green markers represent the points at which the field variables are probed for the grid independence study.

B. Numerical simulation

Two dimensional numerical simulations are carried out for the generated grid using open source SU2 suite [15]. Compressible steady Reynolds Averaged Navier-Stokes (RANS) equations are solved for the flow domain with initial boundary conditions chosen to suitably replicate the actual field variables. An Implicit Euler scheme is set to meet results with residual of 10^{-6}, and a Lower-Upper Symmetric-Gauss-Seidel (LU-SGS) method is used to increase the convergence speed of the code. The boundary conditions, no slip wall and farfield, are fixed based on this history of velocity profile local to the area obtained from National Weather Services [13].

Throughout the year, the velocity of the wind around Boston is between 3 m/s to 12 m/s [13]. Flow simulations are performed by varying the magnitude of inlet velocities (at constant angle) in this recorded range. It is also crucial to account for the changing directions of the wind field throughout the day. We have generated a set of test cases with varying inlet velocity angles and magnitudes. 35 test cases of varying incoming velocity magnitudes (Mach numbers from 0.001 to 0.035 in the intervals of 0.001) at constant heading of zero degree and 23 cases of inlet angles (between

	Monotonic Convergence		Oscillatory Convergence	
N_1, N_2, N_3	Point1	Point2	Point3	Point4
θ_1	0.0118	0.0096	0.0255	0.0273
θ_2	0.0119	0.0094	0.0254	0.0274
θ_3	0.0125	0.0089	0.0253	0.0270
p	0.3736	0.8812	2.121	0.4435
θ_{ext}	0.0122	0.0102	0.0256	0.0270
e_a	0.40%	2.296%	0.65%	0.23%
GCI	3.12%	6.68%	0.11%	1.47%

Table 1 Calculation of Grid Convergence Index using the guidelines drafted in [21]. The extrapolated error in the field variables are calculated to estimate the GCI of the grid.

0° to 115° in the intervals of 5°) at constant Mach number of 0.035 are generated leading to a total of 58 cases.

C. Grid Independence Study

Next we investigate the robustness of the grid. We follow established procedures [21] to calculate the the Grid Convergence Index (GCI), a direct indicator of the quality of the grid. Three meshes (N_1, N_2, N_3) of grid refinement factor r_p = 1.5 (the grids are refined as per the guidelines in [20]) are considered for the study, and Table 1 summarizes the calculations involved in finding the GCI of the three meshes. Five different probe points, Point 1-5 (two upstream and downstream) are chosen in such a way that all critical flow physics are considered. These points are marked with green dots in Figure 3. For the three meshes N_1, N_2, N_3, the field variables $\theta_1, \theta_2, \theta_3$ are probed at a point Point(x)(here x = 1,2,3,4,5).The field variable chosen for our case is Mach number. The GCI is calculated using the Equation 10

$$GCI = \frac{1.25 e_a}{r^p - 1}. \tag{10}$$

D. Validation

The guidelines by the working group at Architectural Institute of Japan [20] suggest that at least one test case of the flow around a single building in an urban area must be validated. For these purposes we use wind velocity data provided by the National Weather Service Forecast office [13], at a station near the region of study. A simulation of the flow in this area is provided in Figure 4. Since the data from the Forecast office is localized and lies inside the urban canopy of turbulent layer, a global average of wind field can be found at [22] to initialize the boundary conditions. The difference between the actual and estimated flow is calculated to be around 8-16%, an acceptable amount given the steady state simulation of an unsteady phenomenon.

V. Path Planning and results

To demonstrate the application of our dataset to path planning, we consider fixed altitude path planning of a UAV traveling at a constant ground speed of 5 m/s.

A. Setup

From the CFD simulation, we obtain the wind velocities at each node of the graph. Then the airspeed is calculated using Equation 3, and a path is found using Dijkstra's algorithm on a weighted graph with weights specified by Equation (9). The values of K_{nav} and K_e are chosen using trial and error to demonstrate the difference between shortest-distance and energy-optimal paths.

These parameters were chosen on the following basis. The value of K_{nav} can neither be 0 nor 1 as they either consider energy required for the flight or the navigation energy at a time respectively and not the both. As our objective is to derive energy optimized paths that also switches between the energy required for navigating to the next waypoint and the air relative energy, the value of K_e should be $K_e < 0.5$ and $K_e > 0.5$ and the values 0 and 1 are indeed incompatible.

Fig. 4 A region in the city of Boston where a local ground station (denoted as '72') is located (left) and the simulated flow used to validate the CFD model (right)

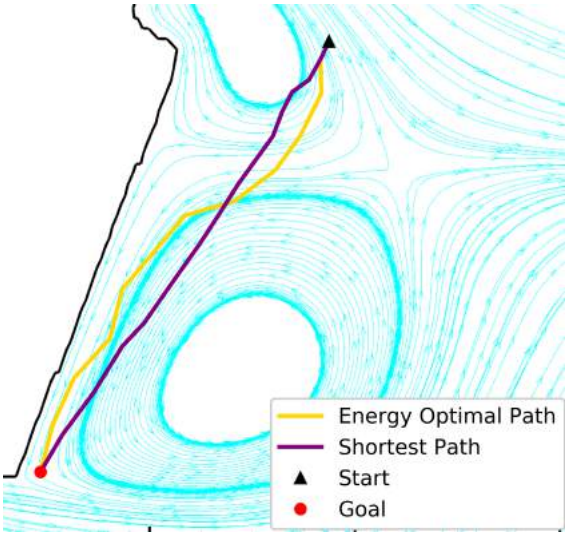

(a) Path traversed by the UAV along the vortex localized behind a building.

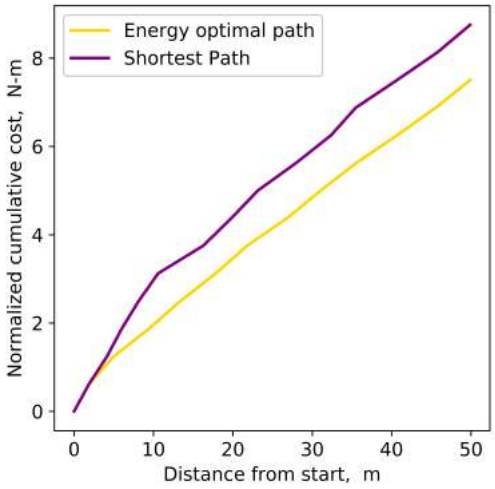

(b) The cumulative cost R as in Equation 9 incurred by the weighted path and the euclidean shortest path.

Fig. 5 Figures (a) and (b) show the path generated and the plot of the cost incurred behind one building respectively.

Comparing the energy gained from the wind field between $K_e = 0.2$ and $K_e = 0.8$, we found that the energy gain is slightly higher for the former case. Furthermore, at $K_e = 0.8$ the switching cost function favors the navigation cost rather than the drag cost at times when the energy to goal is lesser than the energy to the next waypoint. Since our aim is to extract maximum energy from the ambient air while tracking a distance to goal optimized path, we choose to use $K_e < 0.5$.

B. Results

Figure 5 shows the behavior of the UAV following the path generated by the algorithm behind a building with a vortex ring attached to it. The cost incurred at each stage along the path is calculated in both the cases, and Figure 5(b) shows the plot comparing the cumulative cost of the energy optimal path and the shortest path. It indicates that the

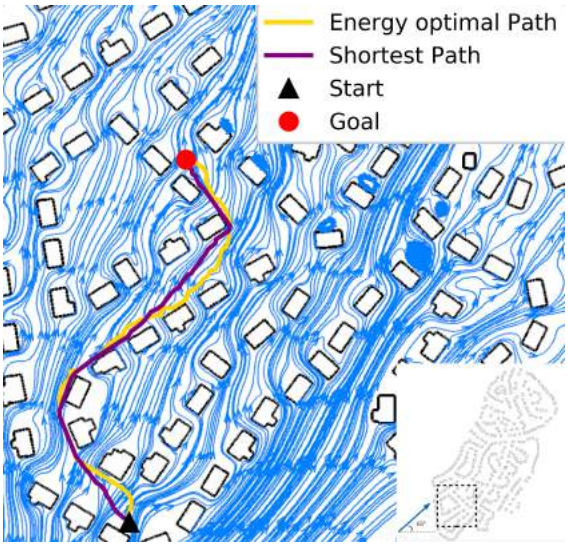

(a) Path generated towards a goal when the wind is in favor of the flight path

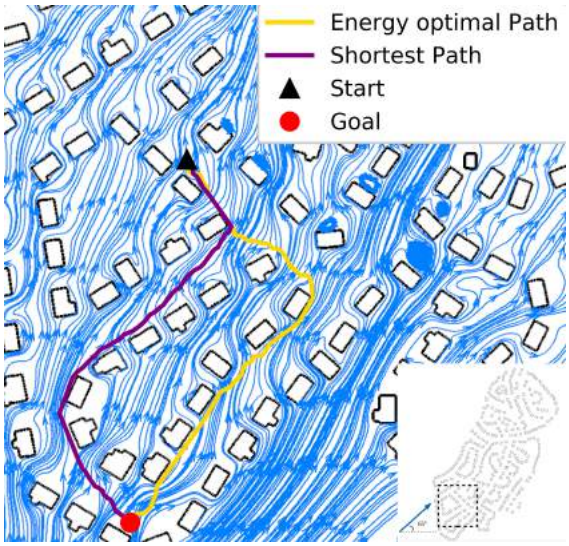

(b) Path generated towards a goal when the wind is against the flight path

Fig. 6 Figures (a) and (b) depict the nature of the paths generated between two setpoints with the start and goal points swapped (in (b)) when the south west wind is blowing at 65° angle.

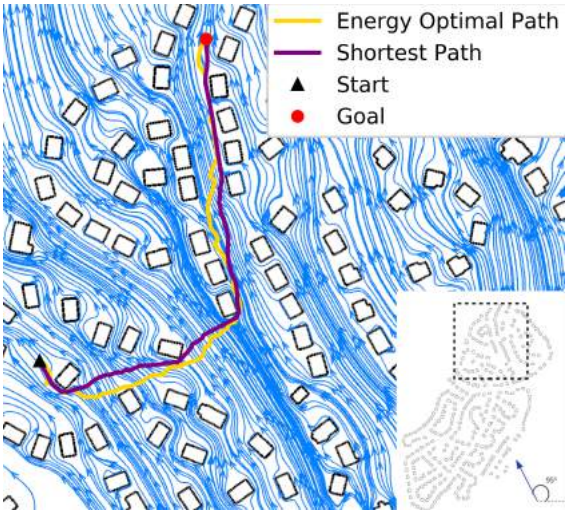

(a) Path generated for a goal point downstream

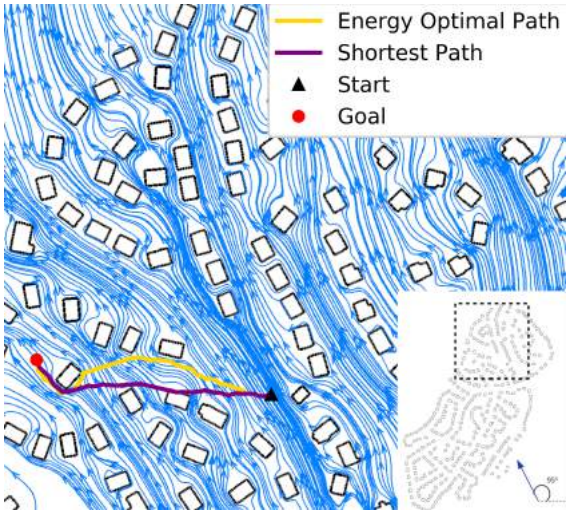

(b) Path generated for a goal point upstream

Fig. 7 Figures (a) and (b) display the paths generated in a region with south east winds blowing at 95° angle.

higher cost in navigating the shortest path can be accounted to the entry of the UAV inside the vortex ring. In practice, this phenomena may even suffer higher energy losses when sudden gusts pushes the UAV more towards the interior of the vortex ring.

Figure 6(a) shows the traversal of a drone towards the goal located downstream the wind field. Here the energy-optimal path is similar to the shortest-distance path. In contrast to Figure 6(a), Figure 6(b) shows the traversal of the drone between the same pair of points, with the difference being that the goal and the start are now interchanged such that the goal lies upstream the wind field such that the UAV needs to travel against the wind. As intended, the energy efficient path in this case significantly differs from the shortest-distance path.

Furthermore, Figure 7 suggests that for goals located downstream of the flow, the optimal path generated is nearly similar to the shortest path, whereas for cases where the goal is located upstream, the flow is disparate. This can be

accounted for by the rise in the drag force experienced by the vehicle when it moves against the wind which in turn reduces the R_{energy} term in the cumulative cost function in Equation 9. The cumulative cost for the energy-optimal path is found to be 22% lesser than the cost incurred in tracking the shortest path.

VI. Conclusion

The primary goal of this work is to advance our understanding of flow physics on path planning in the context of low-level flight by UAVs in urban environments. To this end we generated a dataset of two-dimensional wind fields at varying inlet angles and Mach numbers for a prototypical urban environment using an open-source flow solver. We hope that this dataset will enable other researchers to test their path planning algorithms and to gain an understanding of the challenges involved.

Moreover, we envision that this dataset can be used for other purposes, such as training reduced order models and testing flow-reconstruction algorithms. Another application can consider optimal sensor placement to optimally reconstruct a wind field from localized measurements. We will consider these and other applications in future works.

Appendix

The computationally simulated flow data for all the test cases can be accessed at https://doi.org/10.7302/pdcv-0x63 and at https://www.alexgorodetsky.com/publications/.

Acknowledgment

This work has been funded in part under the DARPA program on Physics of AI, and in part by the Computational Mathematics Program of the AFOSR (P.M. Fariba Fahroo).

References

[1] Markets, and Markets, "Urban Air Mobility Market," `https://www.marketsandmarkets.com/Market-Reports/urban-air-mobility-market-251142860.html`, 2019. [Online; accessed 07-November-2019].

[2] David Gross, P. C. G. F., Steve Rasmussen, "Cooperative Operations in Urban Terrain (COUNTER)," *Defense and Security Symposium*, Orlando, Florida, USA, 2006, pp. 62490G–62490G – 11.

[3] Galway, D., and Etele, J., "Modeling of Urban Wind Field Effects on Unmanned Rotorcraft Flight," *Journal of Aircraft*, Vol. 48, No. 5, 2011, pp. 1613–1620.

[4] "Ampyx," `https://www.ampyxpower.com/`, 2019. [Online; accessed 07-November-2019].

[5] Rayleigh, L., "The Soaring of Birds," *Nature*, Vol. 27, 1883, pp. 534–535.

[6] Allen, M. J., "Autonomous Soaring for Improved Endurance of a SmallUninhabited Air Vehicle," *43rd AIAA Aerospace Sciences Meeting and Exhibit*, Reno, Nevada, USA, 2005, p. 1025 – 1037.

[7] Matthew W. Orr, E. D. K., Steven J. Rasmussen, and Blake, W. B., "Framework for Developing and Evaluating MAV Control Algorithms in a Realistic Urban Setting," *American Control Conference*, Portland, OR, USA, 2005, pp. 4096 –4101.

[8] Lawrance, N. R., and Sukkarieh, S., "Wind Energy Based Path Planning for a Small Gliding Unmanned Aerial Vehicle," *AIAA Guidance, Navigation, and Control Conference*, Chicago, Illinois, 2009, pp. 6112–6129.

[9] Ware, J., and Roy, N., "An Analysis of Wind Field Estimation and Exploitation for Quadrotor Flight in the Urban Canopy Layer," *International Conference on Robotics and Automation (ICRA)*, Stockholm, Sweden, 2016, pp. 16–21.

[10] David Galway, J. E., and Fusina, G., "Development and implementation of an urban wind field database for aircraft flight simulation," *Journal of Wind Engineering and Industrial Aerodynamics*, Vol. 103, 2012, pp. 73–85.

[11] B.Z.Cybyk, T. F. D., B.E.McGrath, and J.F.Keane, "Unsteady Airflows and Their Impact on Small Unmanned Air Systems in Urban Environments," *Journal of Aerospace Information Systems*, Vol. 11, No. 4, 2014, pp. 178–194.

[12] Baskar, D., and Gorodetsky, A., "A Simulated Wind-field Dataset for Testing Energy Efficient Path-Planning Algorithms for UAVs in Urban Environment [Data set]. University of Michigan - Deep Blue." , 2019. https://doi.org/https://doi.org/10.7302/pdcv-0x63.

[13] Service, N. W., "Local Weather Station Data," https://www.wrh.noaa.gov/map, 2019. [Online; accessed 25-July-2019].

[14] "QUIC-CFD, Los Alamos Laboratory," https://www.lanl.gov/projects/quic/reports.shtml, 2019. [Online; accessed 07-November-2019].

[15] Palacios, D. F., and Economon, D. T. D., "SU2 software," https://su2code.github.io/, 2012. [Online; accessed 12-September-2019].

[16] Karaman, S., and Frazzoli, E., "Sampling-based algorithms for optimal motion planning," *The International Journal of Robotics Research*, Vol. 30, No. 7, 2011, pp. 846–894.

[17] "Boston Planning and Development Agency," http://www.bostonplans.org/document-center?doctype=15, 2019. [Online; accessed 25-February-2019].

[18] "CAD Software | 2D And 3D Computer-Aided Design | Autodesk." , Autodesk.com. N.p., 2015. Web. 15 Sept. 2015.

[19] "Pointwise, software package, Version 18, Pointwise, Inc., Fort Worth, Texas, 2017. Pointwise is a registered trademark of Pointwise, Inc. in the USA and the EU," , 2018.

[20] Yoshihide Tominaga, R. Y. H. K. T. N. M. Y. T. S., Akashi Mochida, "AIJ guidelines for practical applications of CFD to pedestrian wind environment around buildings," *Wind Engineering and Industrial Aerodynamics*, Vol. 96, 2008, pp. 1749–1761.

[21] Ismail B. Celik, P. J. R., Urmila Ghia, and Freitas, C. J., "Procedure for Estimation and Reporting of Uncertainty Due to Discretization in CFD Applications," *Journal of Fluids Engineering, Transactions of the ASME*, Vol. 130, No. 7, 2008, p. 780011 – 780014.

[22] "Global Wind data, Weather Flow Inc," https://www.windalert.com/map#44.753,-85.982,11,1,!934, 2019. [Online; accessed 25-July-2019].